Structural Engineering and Mechanics, *Vol. 65, No. 3 (2018) 223-231*
DOI: https://doi.org/10.12989/sem.2018.65.3.223

Numerical investigation on the structural behavior of two-way slabs reinforced with low ductility steel

Zafer Sakka*[1] and R. Ian Gilbert[2a]

[1]*Energy and Building Research Center, KISR, P.O. Box 24885 Safat 13109, Kuwait*
[2]*School of Civil and Environmental Engineering, UNSW, Sydney, Australia*

(Received June 7, 2017, Revised November 1, 2017, Accepted November 28, 2017)

Abstract. A numerical investigation of the impact of steel ductility on the strength and ductility of two-way corner and edge-supported concrete slabs containing low ductility welded wire fabric is presented. A finite element model was developed for the investigation and the results of a series of concurrent laboratory experiments were used to validate the numerical solution. A parametric investigation was conducted using the numerical model to investigate the various factors that influence the structural behavior at the strength limit state. Different values of steel uniform elongation and ultimate to yield strength ratios were considered. The results are presented and evaluated, with emphasis on the strength, ductility, and failure mode of the slabs. It was found that the ductility of the flexural reinforcement has a significant impact on the ultimate load behavior of two-way corner-supported slabs, particularly when the reinforcement was in the form of cold drawn welded wire fabric. However, the impact of the low ductility WWF has showed to be less prominent in structural slabs with higher levels of structural indeterminacy. The load-deflection curves of corner-supported slabs containing low ductility WWF are brittle, and the slabs have little ability to undergo plastic deformation at peak load.

Keywords: ductility; reinforced concrete slabs; low ductility reinforcement; strength; strain localization

1. Introduction

Ductility is a measure of the ability of a structural element or system to sustain plastic deformations before collapse, without substantial loss of load resistance (Warner *et al.* 1998). Ductility is an essential property of concrete structures, and many of the assumptions made routinely in their analysis and design depend on the structure being ductile. Ductility allows for redistribution of internal forces from highly stressed regions to less stressed areas, so that structures can develop the full strength of the critical sections considered in design. On the other hand, brittle structures may not be able to do so. Ductile structures experience relatively large deformations before failure, and this provides warning of impending failure prior to collapse. Ductility also provides robustness and resilience in dissipating the internal energy generated by loading.

The trend in the construction industry to provide more cost-effective materials has led to the use of higher strength reinforcing steel and concrete, fiber reinforced polymers (FRP), fiber reinforcement and high-strength strands. Unfortunately, the use of such materials often has an adverse impact on the ductility of reinforced concrete structures (Ho Park 2017, Bank 2013, Ma *et al.* 2016, Mousa 2015, Wang and Belarbi 2011, Dancygier and Berkover 2016, Sakka 2009, Mohammadhassani *et al.* 2013).

In Australia (Standards Australia 2009), reinforcing steels are classified as either Class N (normal ductility) or Class L (low ductility). For each class of reinforcement, minimum limits are set for the strain at peak stress (or uniform elongation, ε_{su}) and the ratio of tensile strength to yield stress (f_{su}/f_{sy}). For Class L reinforcement, ε_{su} = 1.5% and f_{su}/f_{sy} = 1.03. These limits are considerably lower than the corresponding limits set in any other design code.

Concrete slabs usually have small flexural reinforcement ratios and are generally considered to be very ductile structural members. However, the use of low ductility reinforcing steel in the form of welded wire mesh in one-way slabs loaded to failure has been shown to produce sudden and catastrophic failures caused by fracturing of the tensile reinforcement with very little plastic deformation prior to collapse (Gilbert 2005, Gilbert and Smith 2006, Gilbert and Sakka 2007, Gilbert *et al.* 2006, 2007, Sakka and Gilbert 2008a, Sakka and Gilbert 2008c, Gilbert and Sakka 2009, Gilbert and Sakka 2010, Munter and Patrick 2012a, 2012b). As a result of this work, the Australian Standard AS3600-2009 reduced the strength reduction factor for flexural elements from ϕ = 0.8 for members containing normal ductility steel reinforcement (with $\varepsilon_{su} \geq 5\%$) to ϕ = 0.64 for member containing low-ductility (Class L) reinforcement. This decision has been vindicated for one-way slabs by subsequent experimental and theoretical work (Foster and Kilpatrick 2008, Sakka and Gilbert 2008a, 2008b, 2008c, Goldsworthy *et al.* 2009, Tuladhar and Lancini 2014).

This paper presents a numerical model that was developed for predicting the ultimate load behavior of slabs containing low ductility reinforcement. The model was

*Corresponding author, Associate Research Scientist
E-mail: zsakka@kisr.edu.kw
[a]Emeritus Professor
E-mail: i.gilbert@unsw.edu.au

ISSN: 1225-4568 (Print), 1598-6217 (Online)

calibrated using the results of laboratory tested two-way slabs. A parametric investigation was conducted to investigate the various factors influencing the structural behavior of two-way slabs at the strength limit state. Different values of steel uniform elongation (ε_{su}) and ultimate to yield strength ratios (f_{su}/f_{sy}) are considered. Two types of boundary conditions were considered; corner and edge-supported slabs. Recommendations on the minimum ductility limits for reinforcement used in two-way slabs are also presented.

2. Finite element model

The commercially available finite element software ATENA is used for the numerical analysis. The fracture-plastic constitutive model is used in developing the numerical model for the two-way concrete slabs. The model combines constitutive models for concrete in tension (fracturing) and concrete in compression (plastic behavior). The fracture model is based on the classical orthotropic smeared crack formulation and crack band model. The model employs Rankine failure criterion for concrete cracking. The hardening/softening plasticity model is based on Menetrey-Willam failure surface (Menetrey and Willam 1995). The model uses a return mapping algorithm for the integration of constitutive equations. The method of strain decomposition, as introduced by De Borst (1986), was used to combine fracture and plasticity models. Both models were developed within the framework of the return mapping algorithm proposed by Wilkins (1964).

2.1 Material model formulations

2.1.1 Rankine-fracturing model for concrete cracking

The Rankine-Fracturing model for concrete cracking assumes that strains and stresses are transformed into the material directions. In the case of fixed crack model, strains and stresses are given in the principal directions at the onset of cracking. The Rankine criterion is shown in Eq. (1), and the trial stress is computed by the elastic predictor shown in Eq. (2).

$$F_i^f = \sigma_{ii}^{'t} - f_{ti}^{'} \le 0 \tag{1}$$

$$\sigma_{ij}^{'t} = \sigma_{ij}^{'n-1} + E_{ijkl}\Delta\varepsilon_{kl}^{'} \tag{2}$$

where $\sigma_{ii}^{'t}$ identifies the trial stress, and $f_{ti}^{'}$ the tensile strength in the material direction i and the prime denotes quantities in the material directions.

If the trial stress does not satisfy Eq. (1), the increment of fracturing strain in direction i is computed, assuming that the final stress state satisfies Eq. (3). Eq. (3) can be simplified by assuming that the increment of fracturing strain is normal to the failure surface and that only one failure surface k is checked. In this case, the strain increment can be expressed as shown in Eq. (4) and after the substitution into Eq. (3), a formula for the increment of the fracturing multiplier λ is derived and shown in Eq. (5). This equation is solved by iterations where the material tensile strength $f_t^{'}\left(w_k^{\max}\right)$ is a function of crack opening, w.

$$F_i^f = \sigma_{ii}^{'n} - f_{ti}^{'} = \sigma_{ii}^{'t} - E_{iikl}\Delta\varepsilon_{kl}^{'f} - f_{ti}^{'} = 0 \tag{3}$$

$$\Delta\varepsilon_{ij}^{'f} = \Delta\lambda\frac{\partial F_k^f}{\partial\sigma_{ij}} = \Delta\lambda\delta_{ik} \tag{4}$$

$$\Delta\lambda = \frac{\sigma_{kk}^{'t} - f_{tk}^{'}}{E_{kkkk}} = \frac{\sigma_{kk}^{'t} - f_t^{'}\left(w_k^{\max}\right)}{E_{kkkk}} \tag{5}$$

where w is crack opening, $w_t^{\max} = L_t\left(\hat{\varepsilon}_{kk}^{'f} + \Delta\lambda\right)$, $\hat{\varepsilon}_{kk}^{'f}$ is the total fracturing strain in direction k, $\Delta\lambda$ is the increment in fracturing strain; and L_t is the characteristic length. In ATENA, the crack band size L_t is calculated as the size of the element projected into the crack direction as shown in Fig. 1 (Bazant and Oh 1983, Cervenka *et al.* 1995).

2.1.2 Plasticity model for concrete crushing

In the plastic model, the stress state is computed using Eq. (6). The plastic corrector σ_{ij}^p is computed from the yield function shown in Eq. (7). The return direction l_{ij} in Eq. (7). is defined as shown in Eq. (8). Menetrey-William failure surface is expressed using Eq. (9).

$$\sigma_{ij}^n = \sigma_{ij}^{n-1} + E_{iikl}\left(\Delta\varepsilon_{kl} - \Delta\varepsilon_{kl}^p\right) = \sigma_{ij}^t - E_{iikl}\Delta\varepsilon_{kl}^p = \sigma_{ij}^t - \sigma_{ij}^p \tag{6}$$

$$F^p\left(\sigma_{ij}^t - \sigma_{ij}^p\right) = F^p\left(\sigma_{ij}^t - \Delta\lambda l_{ij}\right) = 0 \tag{7}$$

$$l_{ij} = E_{ijkl}\frac{\partial G^p\left(\sigma_{kl}^t\right)}{\partial\sigma_{kl}} \quad \text{and} \quad \Delta\varepsilon_{ij}^p = \Delta\lambda\frac{\partial G^p\left(\sigma_{ij}^t\right)}{\partial\sigma_{ij}} \tag{8}$$

$$F_{3P}^p = \left(\sqrt{1.5}\frac{\rho}{f_c^{'}}\right)^2 + m\left(\frac{\rho}{\sqrt{6}f_c^{'}}r(\theta,e) + \frac{\xi}{\sqrt{3}f_c^{'}}\right) - c = 0 \tag{9}$$

where $G(\sigma_{ij})$ is the plastic potential function and

$$m = \sqrt{3}\frac{f_c^{'2} - f_t^{'2}}{f_c^{'}f_t^{'}}\frac{e}{e+1} \quad \text{and}$$

$$r(\theta,e) = \frac{4\left(1-e^2\right)\cos^2\theta + (2e-1)^2}{2\left(1-e^2\right)\cos\theta + (2e-1)\left[4\left(1-e^2\right)\cos^2\theta + 5e^2 - 4e\right]^{0.5}}$$

where (ξ, ρ, θ) are Heigh-Vestergaard coordinates; $f_c^{'}$ and $f_t^{'}$ are the concrete compressive and tensile strength, respectively and e is a parameter that defines the roundness of the failure surface $\in\langle 0.5,1.0\rangle$.

2.1.3 Concrete combined model

In the combined model, plasticity is used for concrete crushing and the Rankine fracture model is used for concrete cracking. Two sets of simultaneous inequalities are solved for plastic and fracture strains as shown in Eq. (10).

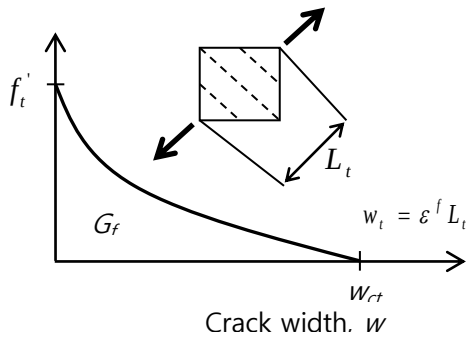

Fig. 1 Tension softening and characteristic length

$$F^p\left(\sigma_{ij}^{n-1} + E_{ijkl}\left(\Delta\varepsilon_{kl} - \Delta\varepsilon_{kl}^f - \Delta\varepsilon_{kl}^p\right)\right) \le 0$$
$$F^f\left(\sigma_{ij}^{n-1} + E_{ijkl}\left(\Delta\varepsilon_{kl} - \Delta\varepsilon_{kl}^p - \Delta\varepsilon_{kl}^f\right)\right) \le 0 \quad (10)$$

2.2 Steel model

The steel reinforcement is modelled using discrete truss elements. A multi-linear stress-strain relationship (Fig. 2) is used in the numerical model. This allows modelling all stages of steel behavior (elastic state, yield plateau, hardening, and fracture). The perfect reinforcement bond model was used to simulate the observed behavior of the test slabs containing Class L WWF. The mechanical anchorage provided by the welded cross-wire in the fabric, coupled with the deformations on the small diameter wires proves to provide outstandingly good bond between the cracked concrete and the longitudinal reinforcing wires. Full details on the computational approach are found in Cervenka *et al.* (2016).

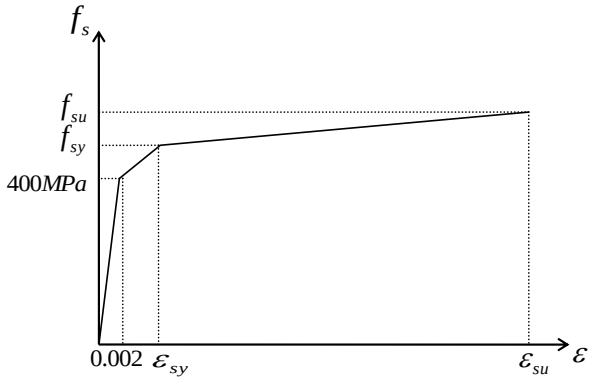

Fig. 2 The multi-linear stress-strain curve used in the model

3. Parametric study

To investigate the impact of steel ductility on the behavior of two-way slabs, a range of different support conditions, aspect ratios (L_x/L_y), steel uniform elongations ε_{su}, and steel ultimate to yield stress ratios f_{su}/f_{sy}, were investigated. Two types of support conditions were investigated as follows:

(i) Panels with free edges and supported at each corner.

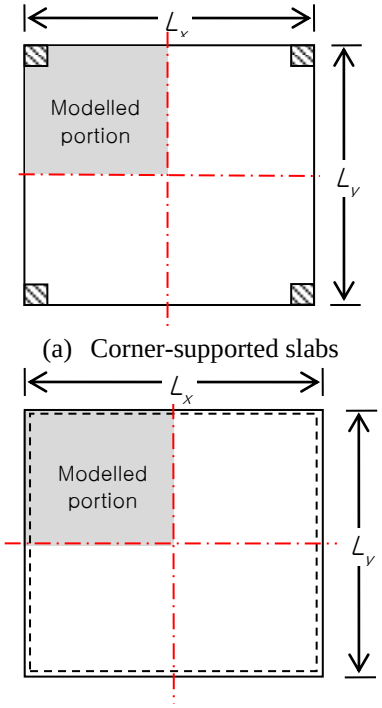

(a) Corner-supported slabs

(b) Edge-supported slabs

Fig. 3 Numerically modelled portion of the slabs using symmetry.

(ii) Panels continuously supported on all four edges.

The structural ductility factor μ can be expressed either by the deflection ratio as expressed in Eq. (11) or by absorbed work ratio as expressed in Eq. (12). In this paper, Eq. (12) is used to measure the ductility.

$$\mu_d = \Delta_u / \Delta_{y1} \quad (11)$$

$$\mu_w = W_1 / W_0 \quad (12)$$

where

μ_d = the ductility factor calculated from deflections;

μ_w = the ductility factor calculated from absorbed work;

Δ_{y1} = the the mid-panel deflection when the first wire yields at the critical section;

Δ_u = the the mid-panel deflection at peak load;

W_0 = the elastic absorbed work;

W_1 = the plastic absorbed work.

Taking advantage of symmetry in the slab geometry, the support conditions and the loading arrangement, it was necessary to model only one-quarter of the slab panel, thereby reducing the size of the numerical problem (Fig. 3). Isoparametric tetrahedral 3-D elements with 4 nodes were used in the finite element model. The plan dimension of each element was typically 50 mm. The element size selection was based on the size that produced convergant results with the fewest number of elements. The 15 mm thick steel plates at the corner support points and at the load application point are modeled as a 3-D elastic isotropic material.

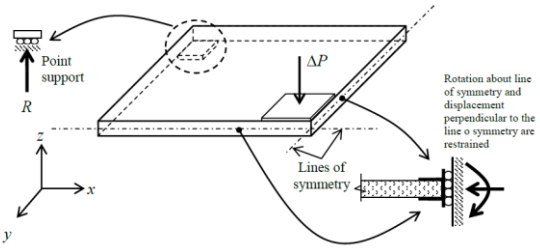

Fig. 4 Boundary conditions at the roller support and lines of symmetry in the corner-supported slabs

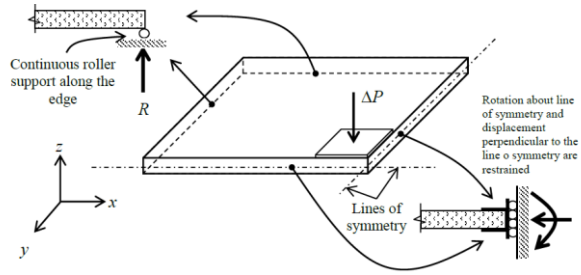

Fig. 5 Boundary conditions at the edges and the lines of symmetry in the edge-supported slabs

Table 1 Load increments used to in the numerical solution

Slab	ΔP (kN)	No. of Steps	ΔP (kN)	No. of Steps	ΔP (kN)	No. of Steps
Corner-supported	1.0	9	0.5	7	0.125	Up to failure
Edge-supported	1.0	16	0.5	6	0.05	Up to failure

Table 2 Dimensions and reinforcement quantities of the quarter panels

Dimensions			Reinforcement					
			x-direction			y-direction		
L_x / 2 (mm)	L_y / 2 (mm)	D (mm)	A_{sx} (mm^2)	d_x (mm)	p (%)	A_{sy} (mm^2)	d_y (mm)	p (%)
Corner-supported slabs								
1,100	1,100	100	6x40=240	85	0.26	6x40=240	79	0.28
1,100	800	100	4x60=240	85	0.35	6x40=240	79	0.28
1,100	1,100	100	4x80=480	85	0.51	6x80=480	79	0.55
1,100	800	100	4x120=480	85	0.71	6x80=480	79	0.55
edge-supported two-way slabs								
1,100	1,100	100	5x40=200	85	0.21	5x40=200	79	0.23
1,100	800	100	4x40=160	85	0.24	5x40=200	79	0.23
1,100	800	100	4x50=200	85	0.29	5x40=200	79	0.23

The boundary conditions of the panels modeled in the investigation are shown in Figs. 4 and 5. Two aspect ratios, namely L_x/L_y = 1.0 (square) and 1.375 (rectangular), were considered for each panel type. All slab panels contained bottom steel in the x and y directions and no top steel. For each support condition and each aspect ratio, four values of steel uniform elongation (1.5%, 2.5%, 5.0% and 8.0%) and two values of ultimate to yield stress ratio (1.03 and 1.05) were investigated. A range of values of bottom steel reinforcement ratios, p (0.21% to 0.71%) were also investigated.

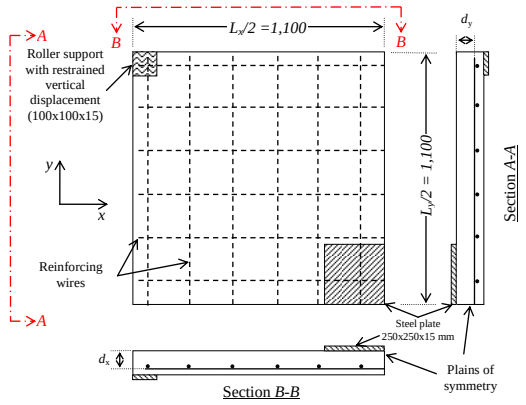

(a) Corner-support square slabs

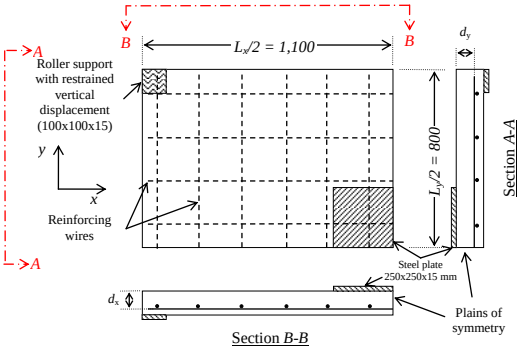

(b) Corner-support rectangular slabs

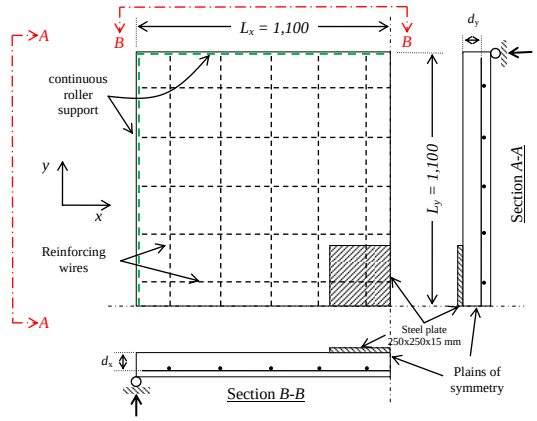

(c) Edge-support square slabs

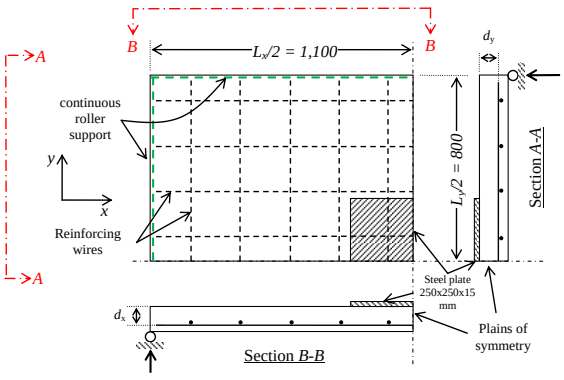

(d) Edge-support square slabs

Fig. 6 Reinforcement layout of the modelled two-way slabs

Table 3 Properties of the corner-supported two-way slab S2S-2

Slab Name	L_y (mm)	L_x (mm)	D (mm)	Steel Class & Type [a]	Bar dia. (mm)	x - direction				y - direction			
						n	A_{stx} (mm^2)	d_x (mm)	p_x (%)	n	A_{sty} (mm^2)	d_y (mm)	p_y (%)
S2S-2	2080	2080	101.4	L - SL82	7.6	12	544	76.2	0.30	12	544	83.8	0.27

[a]L-Class L; N-Class N; n = number of bars or wires

Table 4 Properties of concrete and reinforcement of slab S2S-2

Slab	f'_c (MPa)	ε_c (%)	f_t (MPa)	f_{cf} (MPa)	E_c (GPa)	f_{sy} (MPa)	f_{su} (MPa)	f_{su}/f_{sy}	ε_{su} (%)
S2S-2	44.3	-	3.61	3.87	29.20	600	641	1.07	2.11

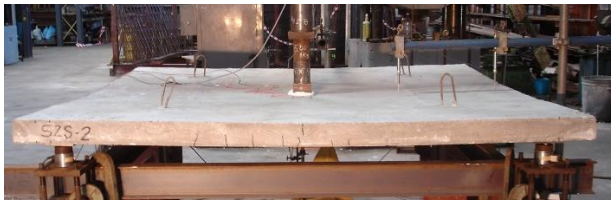

(a) Slab S2S-2 while testing

(b) Slab S2S-2 after collapsing

Fig. 7 Slab S2S-2 during and after the test

Table 5 Comparison between experimental and numerical results

	Experimental	Numerical	Difference (%)
Peak load, P (kN)	65.8	64.3	-2.36
Deflection at peak load, Δ (mm)	30.1	31.6	4.98
Total absorbed Work (kN.mm)	1,620	1,680	3.80

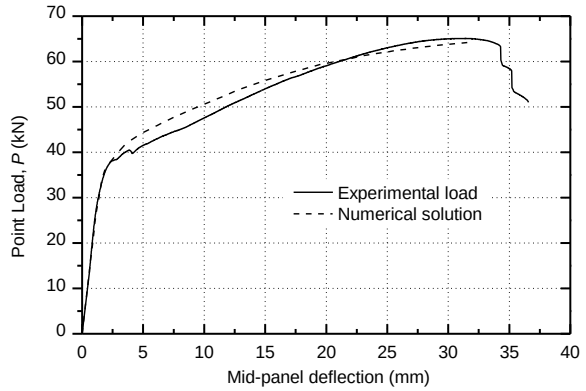

Fig. 8 Experimental versus numerical results for slab S2S-2

Each slab was loaded at the mid-panel by a single point load. The load was applied incrementally up to failure. The load increment was reduced near first cracking and as the peak load was approached in order to accurately capture the load-deflection response at first cracking and at peak loads. Load increments for the corner-supported and edge-supported slabs are listed in Table 1.

The dimensions and reinforcement quantities of the slabs corresponding to the portion of the slab analyzed by the finite element model (i.e., one-quarter of the slab panel) are listed in Table 2 and shown in Fig. 6. In all the models, 250 mm×250 mm×15 mm steel plates were used at the loading point. The plate dimensions at the roller support in Fig. 6 are 100 mm×100 mm×10 mm.

For both types of boundary conditions, the square and rectangular slabs had the same area of reinforcement in both directions. This enabled a direct comparison of the numerical results for the square and rectangular slabs. For the edge-supported slabs, an additional case was examined where the area of secondary reinforcement in the long direction was less than the area of main reinforcement in the short direction. In all the numerical simulations, the reinforcement spacing was kept constant. Four different cross-sectional areas were considered for each of the reinforcing bars (wires): either 40 mm^2, 50 mm^2, 80 mm^2 or 120 mm^2.

4. Calibration of numerical model

The numerical model was calibrated using the results of the laboratory tested two-way slab S2S-2 found in Sakka and Ian (2017) and Sakka (2009). The slab reinforcement details and material properties are shown in Table 3 and Table 4, respectively. Fig. 7 shows the slab during and after testing.

Table 5 and Fig. 8 present a comparison between the experimental and the numerical results for slab S2S-2. The good agreement provides confidence in the results obtained in the subsequent parametric study and the conclusions drawn from them.

5. Numerical results and discussion

In the numerical model, a perfect bond between steel and concrete was assumed and the following concrete materials properties were used:

f_c' = 45.0 MPa; f_t = 3.61 MPa; f_{sy} = 500 MPa; ν = 0.20; ε_c = -2.4×10^{-3}; and E_o = 29.20 GPa

5.1 Corner-supported slabs

Square and rectangular two-way edge-supported slabs were investigated numerically with different values of steel uniform elongation (ε_{su} = 1.5, 2.5, 5.0 or 8.0%) and strength to yield stress ratio (f_{su}/f_{sy} = 1.03 or 1.05). The results of the parametric study for the corner-supported slabs are summarized in Table 6 and Fig. 9 shows the detailed load deflection curves for the case of a square slab with f_{su}/f_{sy} = 1.03, A_{sx} = A_{sy} = 240 mm^2, and f_{sy} = 500 MPa at ε_{su} = 1.5, 2.5, 5.0 and 8.0%. Deflections Δ_{y1} and Δ_{y2} in the figures represent the mid-panel deflections when the first wire yields at the critical section and the mid-panel deflection when all the wires across the critical section yield,

respectively. The deflection Δ_u in the figures correspond to the mid-panel deflection at the peak load. W_0 represents the work done by the applied load in deforming the slab in the elastic range from first loading up until yielding of the first reinforcing wire at a mid-panel deflection of Δ_{y1}. W_1 represents the work done in deforming the slab in the plastic range between the deflection Δ_{y1} and the deflection Δ_u at peak load point. The measure of the ductility of the slab is the ratio W_1/W_0 and this ratio is also given in Table 6.

Table 6 shows that the ultimate load at failure was not significantly affected by ε_{su}. This is due to the determinate nature of the corner-supported slabs, where there are no load paths to transfer additional loads to the supports after the yield of the reinforcement in the critical direction. As the plastic hinge forms (i.e., the yield line across the slab), a failure mechanism develops and strains are localized at the critical section. It can also be seen that the ductility factor increases as the steel uniform elongation ε_{su} increases almost linearly. For any value of ε_{su}, the square slabs have higher ductility factors than the rectangular slabs.

5.2 Edge-supported slabs

Square and rectangular two-way edge-supported slabs were investigated numerically with different values of steel uniform elongation (ε_{su} = 1.5, 2.5, 5.0 or 8.0%) and stress ratio (f_{su}/f_{sy} = 1.03 or 1.05). The results of the parametric study for the edge-supported slabs are summarized in Table 7 and Fig. 10shows the detailed load deflection curves for the case of a square slab with f_{su}/f_{sy} = 1.03, $A_{sx} = A_{sy}$ = 200 mm^2, and f_{sy} = 500 MPa at ε_{su} = 1.5, 2.5, 5.0 and 8.0%. The deflections Δ_y and Δ_u in the figures correspond to the mid-panel deflection when the first reinforcing wire yields and at ultimate load, respectively.

Table 7 lists the yield and peak loads and their associated deflections, load deflection ratios, absorbed work W_0 and W_1, and the ductility factors W_1/W_0. The L_y / Δ ratios listed in Table 7 were calculated based on the shorter span of the slabs (i.e., 2,200 mm for square and 1600 mm for rectangular slabs).

It can be seen from Table 7 that square slabs are a little more ductile than the rectangular slabs and that the ductility factor increases as the steel uniform elongation increases. It is also noted that ductility of the edge-supported slabs is significantly greater than the corner-supported slabs. This is due to high available redundancy in edge-supported slabs. The high redundancy allows loads to transfer from highly stressed areas to less stressed areas, and hence utilizes the reserve strength in these locations in both directions. When the steel in the short direction starts to yield and the flexural strength in that direction is exhausted, additional load can be carried by other load mechanisms including torsion in the slab and membrane action. This makes edge-supported slabs exhibit reasonably ductile behavior even at low values of steel uniform elongation, with significant plastic deformation before the peak load is reached.

Table 7 shows also that the span to deflection ratio L_y/Δ_u decreases when increasing the steel stress ratio f_{su} / f_{sy} which means that the deflection at peak load increases with increasing f_{su} / f_{sy}. The table also shows that the slab ductility increases when increasing steel uniform elongation ε_{su} and stress ratio f_{su} / f_{sy}.

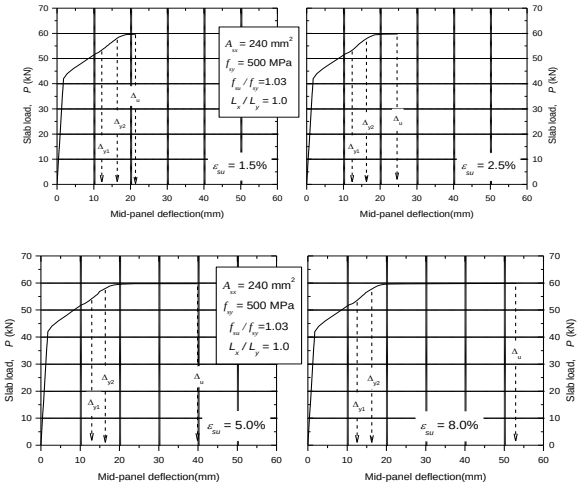

Fig. 9 Load deflection curves and ductility factor for square corner supported slab with $A_{sx} = A_{sy}$ = 240 mm^2, L_x / L_y =1.0, f_{su}/f_{sy}=1.03 and f_{sy} = 500 MPa

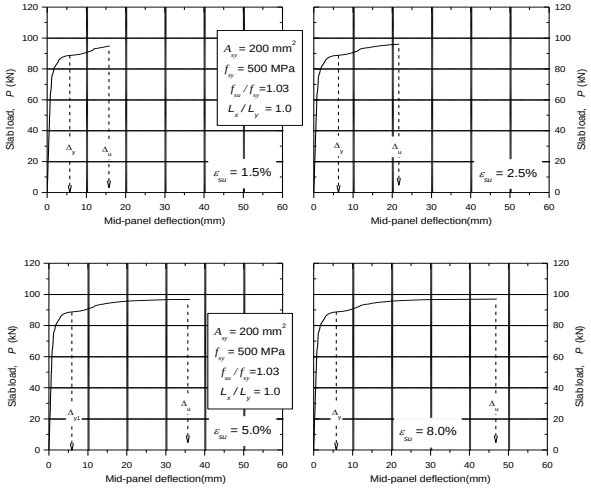

Fig. 10 Load deflection curves and ductility factor for edge-supported slab with $A_{sx} = A_{sy}$ = 200 mm^2, L_x / L_y =1.0, f_{su}/f_{sy}=1.03 and f_{sy} = 500 MPa

In the edge-supported slabs, the applied load started to plateau only after the formation of the plastic hinge (i.e., yield of all the wires across the slab width and the formation of a failure mechanism). For the corner supported slabs, the point at first cracking corresponded to a noticeable kink in the load-deflection curve (i.e., a significant change in direction of the curve), similar to the behavior of one-way slabs reported in Gilbert and Sakka (2010). However, for the edge-supported slabs, the change in direction of the load-deflection curve at first cracking was relatively small, and the loss of stiffness at first cracking was not as significant.

The two different boundary conditions selected for the study represent very different degrees of redundancy. The corner-supported two-way slabs have the least redundancy. In these slabs, the bending moment at mid-span in each direction varied across the slab width, being greatest near the column lines. The reinforcement at the critical section

therefore yielded progressively across the slab width as the applied load approached the peak load. Eventually, all the reinforcements across the weaker direction yielded, and a failure mechanism formed. The mode of failure of a corner-supported two-way slab panel was seen similar to that of a one-way slab. In the case of the edge-supported slabs, a significant part of the load was carried by torsion and in-plane actions, in addition to bending in both orthogonal directions. This created many paths for the applied load to transfer to the continuously supported edges.

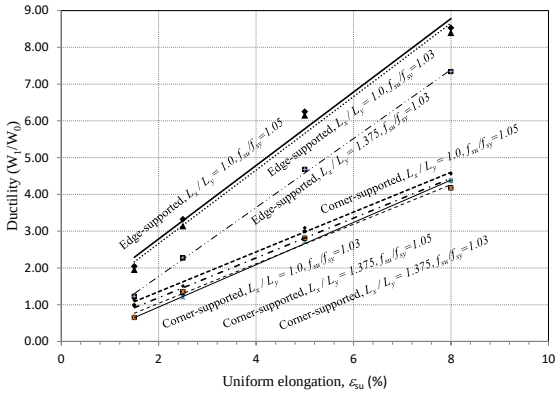

Fig. 11 Ductility ratio (W_1/W_0) versus uniform elongation

Table 6 Yield and peak loads and their associated deflections and absorbed work for corner-supported slabs with f_{sy} = 500 MPa, and A_{sx} = A_{sy} = 240 mm^2

L_x / L_y	f_{su}/f_{sy}	ε_{su}	Δ_{y1} (mm)	P_u (kN)	Δ_u (mm)	W_0 (kN.mm)	W_1 (kN.mm)	W_1/W_0 (kN.mm)
1.0	1.03	1.5	12.3	59.7	21.5	544	535	0.98
		2.5		59.8	24.8	556	717	1.29
		5.0		59.8	39.7	543	1,623	2.99
		8.0		59.8	53.1	552	2,412	4.37
	1.05	1.5	12.4	60.5	23.1	551	622	1.13
		2.5		60.6	26.5	550	829	1.51
		5.0		60.7	40.5	545	1,682	3.09
		8.0		60.8	53.9	544	2,482	4.56
1.375	1.03	1.5	8.37	62.2	13.4	383	247	0.64
		2.5		62.9	16.8	382	459	1.20
		5.0		62.9	26.0	384	1041	2.71
		8.0		62.9	35.8	384	1,677	4.37
	1.05	1.5	8.39	63.3	13.4	382	249	0.65
		2.5		63.8	17.8	386	523	1.35
		5.0		64.0	26.4	385	1081	2.81
		8.0		64.0	34.6	384	1,603	4.17

Fig. 11 shows the ductility ratio W_1/W_0 versus the uniform elongation, ε_{su} for the data in Tables 6 and 7. The figure shows that edge-supported slabs are more ductile than corner-supported slabs. It also shows that the slope of the best fit lines for the edge-supported slabs is higher than the slope of the lines of the corner-supported slabs indicating that the change in the uniform elongation affects the ductility of slabs with high redundancy more than the less redundant slabs. The figure also shows that as the slab aspect ratio L_x/L_y increases (i.e., redundancy decreases), the slab ductility decreases significantly. Furthermore, it can be seen that the slab ductility increases as the stress ratio (f_{su} / f_{sy}) increases. This can be seen for both edge-supported and corner-supported slabs.

Table 7 Yield and peak loads and their associated deflections and absorbed work for edge-supported slabs with A_{sx} = A_{sy} = 200 mm^2, f_{sy} = 500 MPa, and f_{su} / f_{sy} = 1.03

L_x / L_y	f_{su}/f_{sy}	ε_{su} (%)	P_y (kN)	Δ_y (mm)	L_y/Δ_y	P_u (kN)	Δ_u (mm)	L_y/Δ_u	W_0 kN.mm	W_1 kN.mm	W_1/W_0
1.0	1.03	1.5	88.8	6.03	365	94.8	15.95	138	465	909	1.95
		2.5				96.2	21.74	101	465	1,461	3.14
		5.0				96.8	36.24	60.7	465	2,859	6.15
		8.0				97.0	47.03	46.8	465	3,905	8.40
	1.05	1.5	88.8	6.03	365	95.0	16.4	134	465	949	2.04
		2.5				96.4	22.6	97.2	465	1,546	3.32
		5.0				97.2	36.7	59.9	465	2,906	6.25
		8.0				97.4	47.6	46.2	465	3,964	8.52
1.375	1.03	1.5	101.2	4.72	339	105.0	9.77	164	416	511	1.23
		2.5				109.8	13.7	117	416	944	2.27
		5.0				110.0	22.8	70.2	416	1,946	4.68
		8.0				110.0	32.6	49.1	416	3,052	7.34

6. Summary and conclusions

The main conclusions drawn are as follows:

1. The two-way corner supported slabs reinforced with low ductility (Class L) welded wire fabric fail in a brittle mode by fracture of the tensile reinforcement and, generally, not by crushing of the compressive concrete.

2. The current ultimate limit procedures for the design and analysis of reinforced concrete have been developed based on the assumption that the reinforcing steel is elastic-plastic. This is not the case when using low ductiy reinforcing steel and the usual procedures and the conventional understanding of the ultimate load behavior of under-reinforced slabs are not applicable.

3. The uniform elongation of the reinforcement (ε_{su}) has a significant effect on the ductility of two-way reinforced concrete slabs. However, the effect of the reinforcement ductility is much more prominent in the slabs with high reducndancy than those with less reducndancy.

4. The change in slab aspect ratio L_x/L_y affects the ductility of edge-supported slabs much more than the corner-supported slabs.

5. The ductility of the two-way slabs is increased, as the stress ratio (f_{su}/f_{sy}) is increased.

6. The load deflection curves for the corner-supported square and rectangular two-way slabs were unsatisfactorily brittle when ε_{su} < 3.0% and < 4.0%, respectively. These slabs had little ability to undergo significant plastic

deformation at or close to the peak load. In all cases, fracture of the steel occurred at deformations not much larger than the deformation at peak load.

7. The square panels of the corner-supported and edge-supported two-way slabs have higher ductility factors than the rectangular panels.

8. A change in the steel uniform elongation ε_{su} has a higher impact on the ductility factor than a change in the stress ratio f_{su}/f_{sy}.

9. Edge-supported slabs have reasonable ductile behavior even at low values of ε_{su}. This is due to the high redundancy and load transfer by mechanisms other than bending.

Acknowledgments

This study was funded by the Australian Research Council through an ARC Discovery project (DP0558370) and an Australian Professional Fellowship awarded to the second author. The support of the Australian Research Council is gratefully acknowledged.

References

Bank, L.C. (2013), "Progressive failure and ductility of FRP composites for construction: Review", *J. Compos. Constr.*, **17**(3), 406-419.

Bazant, Z.P. and Oh, B.H. (1983), "Crack band theory for fracture of concrete", *Mater. Struct.*, **24**, 155-177.

Cervenka, V., Jendele, L. and Cervenka, J. (2016), *ATENA Program Documentation-Part 1: Theory*, Prague.

Cervenka, V., Pukl, R., Ozbolt, J. and Eligehausen, R. (1995), "Mesh sensitivity effects in smeared finite element analysis of concrete structures", *FRAMCOS 2*, 1387-1396.

Dancygier, A.N. and Berkover, E. (2016), "Cracking localization and reduced ductility in fiber-reinforced concrete beams with low reinforcement ratios", *Eng. Struct.*, **111**, 411-424.

De Borst, R. (1986), "Non-linear analysis of frictional materials", Ph.D. Dissertation, Delft University of Technology, the Netherlands.

Foster, S.J. and Kilpatrick, A.E. (2008), "The use of low ductility welded wire mesh in the design of suspended reinforced concrete slabs", *Austr. J. Struct. Eng.*, **8**(3), 237-248.

Gilbert, R.I. (2005), "Strain localization and ductility of reinforced concrete slabs", *Proceedings of the Australian Structural Engineering Conference*.

Gilbert, R.I. and Sakka, Z.I. (2007), "Effect of reinforcement type on the ductility of suspended reinforced concrete slabs", *J. Struct. Eng.*, **133**(6), 834-843.

Gilbert, R.I. and Sakka, Z.I. (2009), *Effect of Support Settlement on the Strength and Ductility of Reinforced Concrete One-way Slabs Containing Class L Reinforcement*, Concrete 09, Advances and Trends in Structural Engineering, Mechanics and Computation.

Gilbert, R.I. and Sakka, Z.I. (2010), "Strength and ductility of reinforced concrete slabs containing welded wire fabric and subjected to support settlement", *Eng. Struct.*, **32**(6), 1509-1521.

Gilbert, R.I. and Smith, S.T. (2006), "Strain localization and its impact on the ductility of reinforced concrete slabs containing welded wire reinforcement", *J. Adv. Struct. Eng.*, **9**(1), 117-127.

Gilbert, R.I., Sakka, Z.I. and Curry, M. (2006), "Moment redistribution in reinforced concrete slabs containing welded wire fabric", *Proceedings of the 10th East Asia-Pacific Conference on Structural Engineering and Construction*.

Gilbert, R.I., Sakka, Z.I. and Curry, M. (2007), "The ductility of suspended reinforced concrete slabs containing Class L welded wire fabric", *Proceedings of the 19th Australasian Conference on the Mechanics of Structures and Materials*, Christchurch, New Zealand, November-December.

Goldsworthy, H., Siddique, U. and Gravina, R. (2009), "Support settlement and slabs reinforced with low-ductility steel", *ACI Struct. J.*, **106**(6), 840-847.

Ho Park, A.J. (2017), "Ductility analysis of prestressed concrete members with high-strength strands and code implications", *Struct. J.*, **114**(2).

Ma, C., Awang, A.Z. and Omar, W. (2016), "Flexural ductility design of confined high-strength concrete columns: Theoretical modelling", *Measure.*, **78**, 42-48.

Menetrey, P. and Willam, K.J. (1995), "Triaxial failure criterion for concrete and its generalization", *ACI Struct. J.*, **92**(3), 311-318.

Mohammadhassani, M., Suhatril, M., Shariati, M. and Ghanbari, F. (2013), "Ductility and strength assessment of HSC beams with varying of tensile reinforcement ratios", *Struct. Eng. Mech.*, **48**(6), 833-848.

Mousa, M.I. (2015), "Flexural behaviour and ductility of high strength concrete (HSC) beams with tension lap splice", *Alexandr. Eng. J.*, **54**(3), 551-563.

Munter, S. and Patrick, M. (2012a), "SRIA's class L mesh elevated slab tests: Part 1A-objectives, design & details", *Proceedings of the Australian Structural Engineering Conference*, Perth, Australia, July.

Munter, S. and Patrick, M. (2012b), "SRIA's class L mesh elevated slab tests: Part 1B-observations and results", *Proceedings of the Australasian Structural Engineering Conference*, Perth, Australia, July.

Sakka, Z. (2009), "Impact of Steel Ductility on the Structural Behaviour and Strength of RC Slabs", Ph.D. Dissertation, University of New South Wales, Australia.

Sakka, Z.I. and Gilbert, R.I. (2008a), *Effect of Reinforcement Ductility on the Strength and Failure Modes of One-way Reinforced Concrete Slabs*, Rep. No. UNICIV Report R-450, School of Civil and Environmental Engineering, The University of New South Wales, Sydney, Australia.

Sakka, Z.I. and Gilbert, R.I. (2008b), *Effect of Reinforcement Ductility on the Strength, Ductility and Failure Modes of Continuous One-way Concrete Slabs Subjected to Support Settlement-Part 1*, Rep. No. UNICIV Report R-451, School of Civil and Environmental Engineering, The University of New South Wales, Sydney, Australia.

Sakka, Z.I. and Gilbert, R.I. (2008c), *Effect of Reinforcement Ductility on the Strength, Ductility and Failure Modes of Continuous One-way Concrete Slabs Subjected to Support Settlement-Part 2*, Rep. No. UNICIV Report R-452, School of Civil and Environmental Engineering, The University of New South Wales, Sydney, Australia.

Sakka, Z.I. and Ian, G.R. (2017), "Structural behavior of two-way slabs reinforced with low-ductility WWF", *J. Struct. Eng.*, **143**(12), 04017166.

Standards Australia (2009), *Concrete Structures*, AS 3600-09, Sydney, Australia.

Tuladhar, R. and Lancini, B.J. (2014), "Ductility of concrete slabs reinforced with low-ductility welded wire fabric and steel fibers", *Struct. Eng. Mech.*, **49**(4), 449-461.

Wang, H. and Belarbi, A. (2011), "Ductility characteristics of fiber-reinforced-concrete beams reinforced with FRP rebars", *Constr. Build. Mater.*, **25**(5), 2391-2401.

Warner, R.F., Rangan, B.V., Hall, A.S. and Faulkes, K.A. (1998), *Concrete Structures*, Longman, Australia.

Wilkins, M.L. (1964), "Calculation of elastic-plastic flow, methods of computational physics", *Meth. Comput. Phys.*, **3**.

CC